

Dynamical Modeling Based on Energy Dissipation

Pingwen Zhang

School of Mathematical Sciences and CCSE, Peking Univ., China

Joint work with Haijun Yu, Guanghua Ji, Han Wang, Kun Li

April 18, 2007



Dynamical modeling based on energy dissipation

- The elastic stress can be derived from general energy using virtue work principle
- The viscous stress can be derived by understanding dissipation
- The kinematics

The following is our some related works:

- Dongzhuo Zhou, Pingwen Zhang and Weinan E, Modified models of polymer phase separation PHYSICAL REVIEW E 73 (6): Art. No. 061801 Part 1 JUN (2006)
- Dan Hu, Pingwen Zhang and Weinan E, The continuum theory of a moving membrane, PHYSICAL REVIEW E (2007)



Dynamical modeling based on energy dissipation

Bottom up

- The microscopic dynamical model is given
- We hope to get the macroscopic dynamical model

Today, I will focus on

The Thermodynamic Closure Approximation of Kinetic Theories
for Complex Fluids



Contents

Background

- Two approaches to tensor models

- Criteria of good closure approximations

- Quasi-equilibrium closure approximation (QEA)

FENE-QE Model

- FENE-QE model

- Implementation: FENE-QE-PLA

- Numerical results

Nonhomogeneous Kinetic Theories of LCPs

- Review of kinetic theories of LCPs

- Second-order moment model

- Fourth-order moment model

- Issue of implementation

- Numerical results of Bingham closure model

Conclusion and comments



Outline

Background

- Two approaches to tensor models

- Criteria of good closure approximations

- Quasi-equilibrium closure approximation (QEA)

FENE-QE Model

- FENE-QE model

- Implementation: FENE-QE-PLA

- Numerical results

Nonhomogeneous Kinetic Theories of LCPs

- Review of kinetic theories of LCPs

- Second-order moment model

- Fourth-order moment model

- Issue of implementation

- Numerical results of Bingham closure model

Conclusion and comments



Modeling of Complex Fluids

- 1 Continuity theories
 - Oldroyd-B model, Leslie-Ericksen theory etc
 - relatively simple and efficient in numerical simulation
 - only accurate in some special cases
- 2 Kinetic theories or molecular theories
 - FENE model, the Doi kinetic theory etc
 - more accurate than continuity theories
 - computing is expensive in nonhomogeneous system
- 3 **Tensor models**
 - describe local structure by an order tensor
 - a compromise between accuracy and efficiency
 - grab microstructure while serving as constitutive equation



Two approaches to tensor models

1 Landau theory

Define a phenomenological free energy in terms of order parameter or order tensor. For example, the Landau-de Gennes theory for LCPs:

$$A[S] = \frac{1}{V} \int d\mathbf{r} \left[\frac{a}{2} \mathbf{Tr}(S \cdot S) + \frac{b}{2} \mathbf{Tr}(S \cdot S \cdot S) + \frac{1}{4} (\mathbf{Tr}(S \cdot S))^2 + \frac{d}{2} \frac{\partial S_{\alpha\beta}}{\partial x_\gamma} \frac{\partial S_{\alpha\beta}}{\partial x_\gamma} + \frac{e}{2} \frac{\partial S_{\alpha\gamma}}{\partial x_\alpha} \frac{\partial S_{\beta\gamma}}{\partial x_\beta} \right]$$

Then the dynamics of S can be written formally as

$$\frac{dS}{dt} = \nabla \cdot \left(L \cdot \nabla \frac{\partial A}{\partial S} \right) - D(M) \frac{\partial A}{\partial S} + F_{\text{ext}}$$



Two approaches to tensor models

2 Reduced from kinetic theory by **closure approximation**

- the Doi theory for LCPs

$$\frac{df}{dt} = \frac{1}{De} \mathcal{R} \cdot (\mathcal{R}f + f\mathcal{R}U) - \mathcal{R} \cdot (\mathbf{m} \times \kappa \cdot \mathbf{m}f) \quad (1)$$

U is Maier-Saupe potential

$$U(\mathbf{m}, t) = U_0 \int |\mathbf{m} \times \mathbf{m}'|^2 f(\mathbf{m}', t) d\mathbf{m}'$$

multiple $\mathbf{m}\mathbf{m}$ on the both sides of (1) and integrate, one get

$$\frac{dM}{dt} = -\frac{2}{De} \left[(3M - I) + 2U_0(M \cdot M - M : Q) \right] \quad (2)$$

where $M = \langle \mathbf{m}\mathbf{m} \rangle$, $Q = \langle \mathbf{m}\mathbf{m}\mathbf{m}\mathbf{m} \rangle$.



Two approaches to tensor models

- FENE model

$$\frac{df}{dt} = \frac{2}{\xi} \nabla_{\mathbf{q}} \cdot (\nabla_{\mathbf{q}} f + f \nabla_{\mathbf{q}} V) - \nabla_{\mathbf{q}} \cdot (\kappa \cdot \mathbf{q} f) \quad (3)$$

where V is FENE potential

$$V(\mathbf{q}) = -\frac{HQ_0^2}{2} \ln \left(1 - \frac{\mathbf{q}^2}{Q_0^2} \right)$$

the stress introduced by polymer is

$$\tau^e = \langle \mathbf{q} \nabla_{\mathbf{q}} (\ln f + V) \rangle = -I + \left\langle \frac{H\mathbf{q}\mathbf{q}}{1 - \mathbf{q}^2/Q_0^2} \right\rangle$$

multiple $\mathbf{q}\mathbf{q}$ on the both sides of (3) and integrate, one get

$$\frac{dM}{dt} = \kappa \cdot M + M \cdot \kappa - \frac{4}{\xi} \tau^e$$



What's the differences between two approaches?

- Landau theory is phenomenal, ignore some microscopic configuration entropy
- Landau theory ensure energy dissipation in isothermal system
- the second approach need closure approximation, but give more credible results
- not all closure approximations ensure energy dissipation



Choice of closure approximations

Several closures were introduced in the passed thirty years

- quadratic closure (Doi 1981): $Q = MM$
- HL1, HL2 closure approximation (Hinch, Leal 1976) [▶ details](#)
- Bingham closure approximation (Chaubal and Leal 1998)

$$Q = \int \mathbf{m} \mathbf{m} \mathbf{m} \mathbf{m} \frac{1}{Z} \exp(B : \mathbf{m} \mathbf{m}) d\mathbf{m},$$

where $\int \mathbf{m} \mathbf{m} \frac{1}{Z} \exp(B : \mathbf{m} \mathbf{m}) = M.$

- FENE model: FENE-P (Perterlin 1966), FENE-L (LieLens et al 1999) etc
- quasi-equilibrium closure approximation (Ilg et al 2002, 2003)

Which one is better ?



Criteria of good closure approximations

We present four criteria of good closure approximations

- 1 non-negative CDF $f \geq 0$
- 2 energy dissipation in isothermal system

$$T \frac{dS}{dt} = - \frac{d}{dt} \left(\int \frac{1}{2} \rho \mathbf{u} \cdot \mathbf{u} dx + A[M] \right) \geq 0.$$

and consistent with that of exact kinetic theory

- 3 good accuracy of approximation
- 4 low computational expense



Quasi-equilibrium closure approximation (QEA)

Background

Quasi-equilibrium approximation is a basic principle of statistical physics.

- The very first use of the entropy maximization dates back Gibbs' classical work: Elementary Principles of Statistical Mechanics (Dover, 1960).
- The use of the quasi-equilibrium to reduce the description of dissipative system can be traced to the works of Grad on the Boltzmann equation (1949).
- QEA was employed in closure approximation of kinetic theory for flexible and rod-like polymer dynamics by Ilg et al.

P. Ilg, I. V. Karlin, H.C. Öttinger, Canonical distribution functions in polymer dynamics. (I). Dilute solutions of flexible polymers, Physica A 315 (2002)

P. Ilg, I.V. Karlin, M. Kröger, H.C. Öttinger, Canonical distribution functions in polymer dynamics. (II). Liquid-crystalline polymers, Physica A 319 (2003)



Quasi-equilibrium closure approximation (QEA)

Consider a system with free energy

$$A[f] = \int f \ln f + \frac{1}{2} U_f(\mathbf{m}) f + V(\mathbf{m}) f d\mathbf{m}$$

U_f is mean-field potential and V is external potential. Then the dynamics of the system given by

$$\frac{df}{dt} = \nabla_{\mathbf{m}} [D(\mathbf{m}) \cdot \nabla_{\mathbf{m}} \mu], \quad \mu = \frac{\delta A[f]}{\delta f}. \quad (4)$$

The energy dissipation is

$$-\frac{dA[f]}{dt} = -\left(\frac{\delta A}{\delta f}, \frac{df}{dt}\right) = (\nabla \mu, D(\mathbf{m}) \nabla \mu) \geq 0.$$



Quasi-equilibrium closure approximation (QEA)

One can get the dynamics of macro-variables $S_i = \int s_i(\mathbf{m})f(\mathbf{m})d\mathbf{m}$ from equation (4)

$$\frac{dS_i}{dt} = \int s_i(\mathbf{m})\nabla[D(\mathbf{m}) \cdot \nabla\mu]d\mathbf{m}, \quad i = 1, \dots, n. \quad (5)$$

The right sides of (5) usually involves more macro-variables, often are higher order term, How to make it closed?

A basic idea is to close it without introducing more information on distribution function. Thus the higher order macro-variables are ensembled by the most probable distributions, which are obtained by taking maximum entropy or minimum of free energy

$$\begin{aligned} \min \quad & A[f] \\ \text{s.t.} \quad & \int s_i(\mathbf{m})f(\mathbf{m})d\mathbf{m} = S_i, \quad i = 1, \dots, n. \end{aligned}$$



Quasi-equilibrium closure approximation (QEA)

By the method of Lagrange multipliers, we get

$$\mu = \ln f + U_f(\mathbf{m}) + V(\mathbf{m}) = \sum_{i=1}^n \lambda_i s_i(\mathbf{m})$$

Then the quasi-equilibrium distribution reads

$$f = \exp \left(-V(\mathbf{m}) - U_f(\mathbf{m}) + \sum_{i=1}^n \lambda_i s_i(\mathbf{m}) \right).$$

Suppose the relationship of $U_f(\mathbf{m})$ and f are given by

$$U_f(\mathbf{m}) = \sum_{i,j} S_i A_{ij} s_j(\mathbf{m}),$$

where A is a symmetric matrix.



Quasi-equilibrium closure approximation (QEA)

Then

$$f_S(\mathbf{m}) = \exp\left(-V(\mathbf{m}) - \sum_{i,j} S_i A_{ij} s_i(\mathbf{m}) + \sum_i \lambda_i s_i(\mathbf{m})\right),$$

$$\text{where } \int s_i(\mathbf{m}) f_S(\mathbf{m}) d\mathbf{m} = S_i, \quad i = 1, \dots, n.$$

Define the macroscopic free energy by $A[S] = A[f_S]$, then

$$\frac{\partial A[S]}{\partial S_i} = \lambda_i.$$

And the energy dissipation hold for reduced equation (5)

$$\begin{aligned} -\frac{dA[S]}{dt} &= -\sum_i \frac{\partial A[S]}{\partial S_i} \frac{dS_i}{dt} = -\sum_i \lambda_i (s_i(\mathbf{m}), \frac{df}{dt})|_{f=f_S} \\ &= -\left(\sum_i \lambda_i s_i(\mathbf{m}), \nabla D(\mathbf{m}) \nabla \mu\right)|_{f=f_S} = (\nabla \mu, D(\mathbf{m}) \nabla \mu) \geq 0. \end{aligned}$$



Outline

Background

- Two approaches to tensor models

- Criteria of good closure approximations

- Quasi-equilibrium closure approximation (QEA)

FENE-QE Model

- FENE-QE model

- Implementation: FENE-QE-PLA

- Numerical results

Nonhomogeneous Kinetic Theories of LCPs

- Review of kinetic theories of LCPs

- Second-order moment model

- Fourth-order moment model

- Issue of implementation

- Numerical results of Bingham closure model

Conclusion and comments



FENE-QE model

Given second-order moment M , we take the QE distribution

$$f_M(\mathbf{q}) = \frac{1}{Z} \exp(-V(\mathbf{q})) \exp(R : \mathbf{q}\mathbf{q})$$

as the reference CDF to estimate polymer stress

$$\tau^e = \langle \mathbf{q} \nabla_{\mathbf{q}} \mu \rangle = R \cdot M + M \cdot R$$

Then the closed equation reads

$$\frac{dM}{dt} = \kappa \cdot M + M \cdot \kappa - \frac{4}{\xi} (R \cdot M + M \cdot R), \quad (6)$$

where R are determined by $\int \mathbf{q}\mathbf{q} \exp(-V) \exp(R : \mathbf{q}\mathbf{q}) d\mathbf{q} = M$.



FENE-QE model

Equation (6) together with incompressible Navier-Stokes equation

$$\begin{aligned}\frac{d\mathbf{u}}{dt} + \nabla p &= \nabla \cdot \tau^e + \frac{1}{Re} \Delta \mathbf{u} \\ \nabla \cdot \mathbf{u} &= 0.\end{aligned}$$

compose a well-defined system. The energy dissipation of the system reads

$$\begin{aligned}T \frac{dS}{dt} &= -\frac{d}{dt} \left[\int_{\Omega} \frac{1}{2} \rho \nu^2 d\mathbf{x} + A[M] \right] \\ &= \int_{\Omega} \frac{1}{Re} |\nabla \mathbf{u}|^2 d\mathbf{x} + \int_{\Omega} \frac{8}{\xi} Tr(R \cdot M \cdot R) d\mathbf{x} \\ &\geq 0.\end{aligned}$$



Implementation of FENE-QE

Calculate R from M is equal to solving a system of the non-linear equations. Note: Z also depends on R .

$$M = G(R) = \frac{1}{Z} \int \mathbf{q}\mathbf{q} \left[1 - \left(\frac{\mathbf{q}}{Q_0} \right)^2 \right]^{HQ_0^2/2} \exp \{ R : \mathbf{q}\mathbf{q} \} d\mathbf{q}$$

Newtonian iteration:

$$R_{n+1} = R_n - \nabla G(R_n)^{-1} G(R_n), \quad n = 0, 1, 2, \dots \quad (7)$$

Difficulties

- Numerical integration of 2- or 3- dimensional variables.
- Ill posed function to be integrated, when index $HQ_0^2/2$ is small and R is big.



Implementation of FENE-QE

Strategy of Ilg et al

By Legendre transform, the independent variables are changed from M to R

$$\frac{dR}{dt} = (Q - MM)^{-1} : \frac{dM}{dt}.$$

Ilg et al proposed a first-order integration scheme for this equation. It need to evaluate Q and M in each time step.

The computing cost is still expensive for nonhomogeneous system simulation.



Our choice: piecewise linear approximation (PLA) to G^{-1}

M and R can be diagonalized at the same time. So we only consider the case when both M and R are diagonal matrices.

- 1 Generate a grid on the range of G .
- 2 Calculate the value of G^{-1} at each grid point by Newtonian iteration.
- 3 Given any value of M , calculate $G^{-1}(M)$ by linear interpolation of four neighboring grid points



Grid generation

- one-dimensional case

First divide the domain of $G(R)$ into a uniform grid $\{R_0, R_1, \dots, R_N\}$, then evaluate every $G(R_i)$. The series $\{G(R_0), G(R_1), \dots, G(R_n)\}$ gives a grid on the range of $G(R)$.

- two-dimensional case

Tensor product of 1-dimensional grid. The ij^{th} grid point is $\{G(R_i), G(R_j)\}$

Rectangular grids (not necessarily uniform) are usually better than non-rectangular grids. Furthermore, it is easy to carry out bisection search method on rectangular grids.



Numerical results

Numerical comparison of three second-order moment closed FENE models

- FENE-P (Bird et al 1987)

R.B. Bird, C.F. Curtiss, R.C. Armstrong and O. Hassager, Dynamics of Polymeric Liquids, Vol. 2: Kinetic Theory, Wiley, New York, 2nd edn., 1987.

- FENE-QE (Ilg et al 2002)

- FENE-QE-PLA

- FENE-YDL

P. Yu, Q. Du and C. Liu, From micro to macro dynamics via a new closure approximation to the FENE model of polymeric fluids, SIAM J. Multiscale Model. Simul., 3 (2005) 895–917.



Numerical results– steady shear flow

steady shear flow

scheme central difference

fourth-order explicit Runge-Kutta

parameters $\mathbf{u} = (\kappa y, 0)$, $\xi = 40$, $H = 100$ and $Q_0 = 1$



Numerical results– steady shear flow

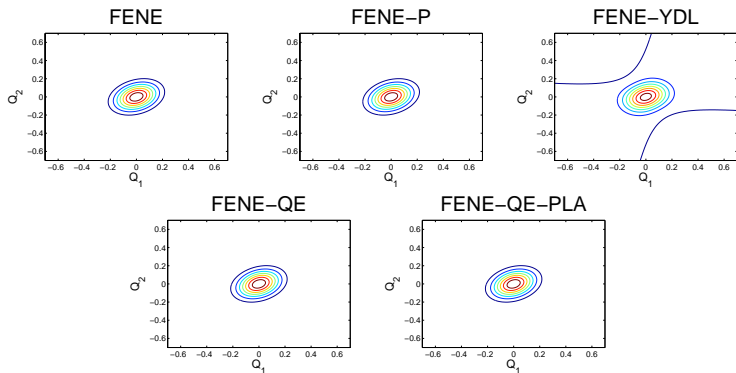


Figure: Comparison of the contour plots of the CDFs at $\kappa = 3$.



Numerical results– steady shear flow

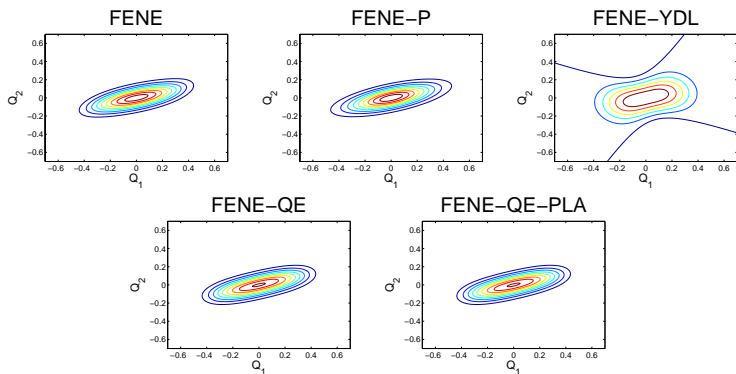


Figure: Comparison of the contour plots of the CDFs at $\kappa = 15$.



Numerical results– steady shear flow

κ	FENE-P	FENE-YDL	FENE-QE	FENE-QE-PLA
1	1.10×10^{-2}	4.02×10^{-3}	4.07×10^{-4}	4.17×10^{-4}
3	1.37×10^{-2}	3.68×10^{-2}	9.45×10^{-4}	9.07×10^{-4}
6	2.21×10^{-2}	1.38×10^{-1}	4.43×10^{-3}	4.24×10^{-3}
9	3.49×10^{-2}	2.72×10^{-1}	1.34×10^{-2}	1.29×10^{-2}
15	6.99×10^{-2}	5.45×10^{-1}	5.73×10^{-2}	5.65×10^{-2}
20	9.97×10^{-2}	7.40×10^{-1}	1.20×10^{-1}	1.19×10^{-1}

Table: L^1 Norm of Error of CDFs



Numerical results– steady shear flow

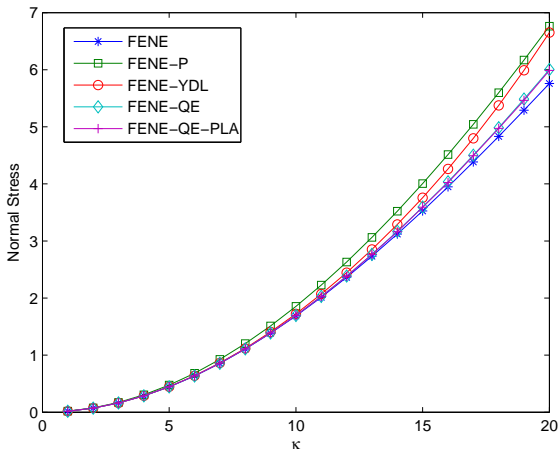


Figure: Comparison of the Normal Stress Difference



Numerical results– steady shear flow

κ	FENE-P	FENE-YDL	FENE-QE	FENE-QE-PLA
1	1.10×10^{-3}	2.08×10^{-6}	7.23×10^{-6}	3.76×10^{-5}
3	1.03×10^{-2}	1.96×10^{-4}	2.66×10^{-5}	2.57×10^{-4}
6	4.79×10^{-2}	3.71×10^{-3}	6.31×10^{-4}	1.05×10^{-3}
9	1.28×10^{-1}	2.23×10^{-2}	5.32×10^{-3}	4.65×10^{-3}
15	4.78×10^{-1}	2.32×10^{-1}	6.68×10^{-2}	6.57×10^{-2}
20	1.00×10^0	8.93×10^{-1}	2.46×10^{-1}	2.31×10^{-1}

Table: Error of the Normal Stress Difference compared to Fokker-Planck equation



Numerical results– steady shear flow

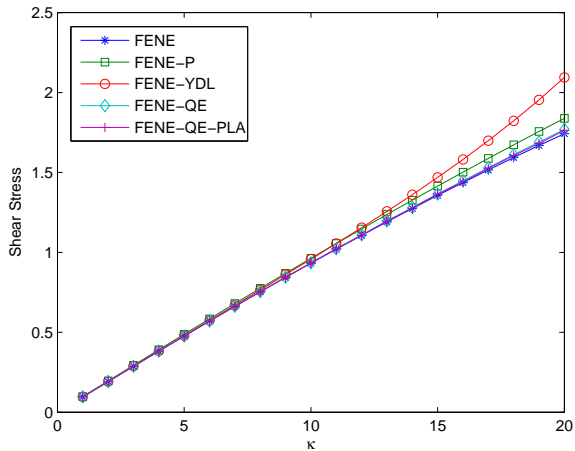


Figure: Comparison of the shear stress.



Numerical results– steady shear flow

κ	FENE-P	FENE-YDL	FENE-QE	FENE-QE-PLA
1	1.90×10^{-3}	1.32×10^{-5}	1.90×10^{-6}	1.35×10^{-5}
3	6.02×10^{-3}	4.35×10^{-4}	7.13×10^{-6}	7.43×10^{-5}
6	1.41×10^{-2}	4.12×10^{-3}	2.17×10^{-4}	3.66×10^{-4}
9	2.54×10^{-2}	1.69×10^{-2}	1.18×10^{-3}	7.67×10^{-4}
15	5.86×10^{-2}	1.13×10^{-1}	9.13×10^{-3}	8.46×10^{-3}
20	9.62×10^{-2}	3.52×10^{-1}	2.72×10^{-2}	2.10×10^{-2}

Table: Error of the Shear Stress compared to Fokker-Planck equation



Numerical results– steady shear flow

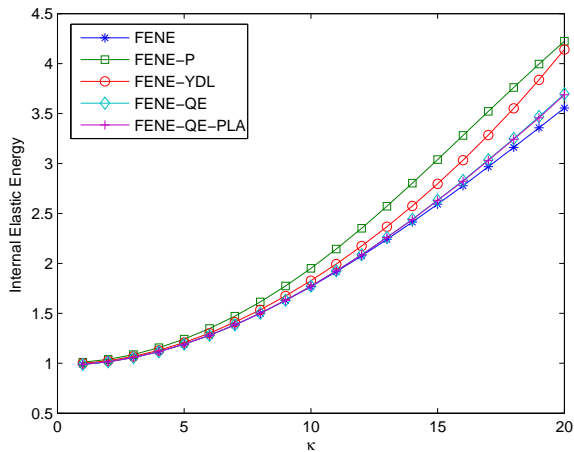


Figure: Comparison of the Elastic Energy



Numerical results– steady shear flow

κ	FENE-P	FENE-YDL	FENE-QE	FENE-QE-PLA
1	2.11×10^{-2}	9.85×10^{-3}	1.30×10^{-5}	1.20×10^{-5}
3	3.03×10^{-2}	1.20×10^{-2}	2.51×10^{-5}	2.74×10^{-5}
6	6.72×10^{-2}	2.16×10^{-2}	3.92×10^{-4}	8.57×10^{-5}
9	1.45×10^{-1}	4.58×10^{-2}	3.23×10^{-3}	1.81×10^{-3}
15	4.47×10^{-1}	2.04×10^{-1}	3.96×10^{-2}	3.88×10^{-2}
20	6.69×10^{-1}	5.85×10^{-1}	1.41×10^{-1}	1.33×10^{-1}

Table: Error of the elastic energy compared to Fokker-Planck equation



Numerical results– elongational flow

elongational flow

$$\mathbf{u} = (\kappa x, -\kappa y)$$



Numerical results– elongational flow

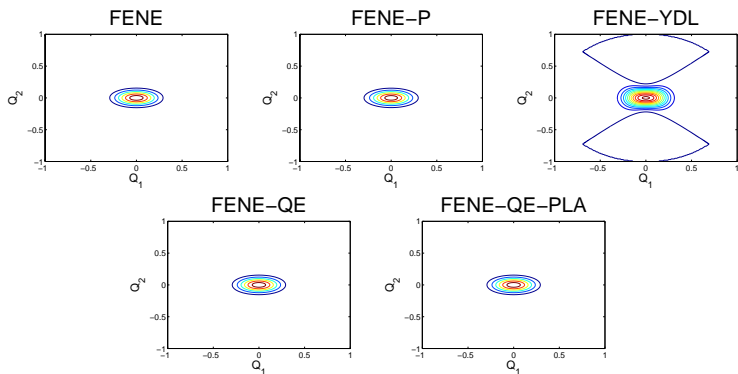


Figure: Contour Plots of CDFs for $\kappa = 3$



Numerical results– elongational flow

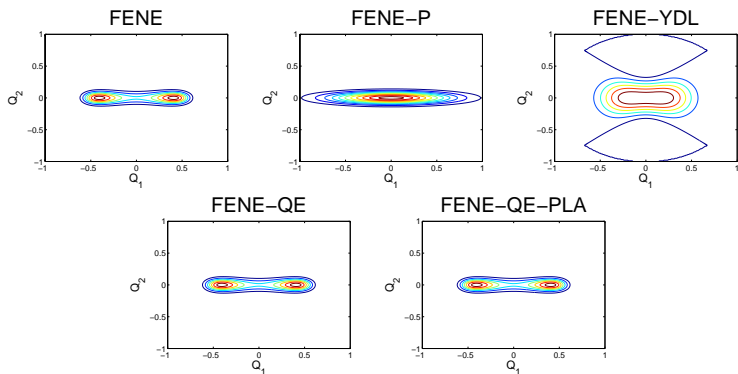


Figure: Contour Plots of CDFs for $\kappa = 6$



Numerical results– elongational flow

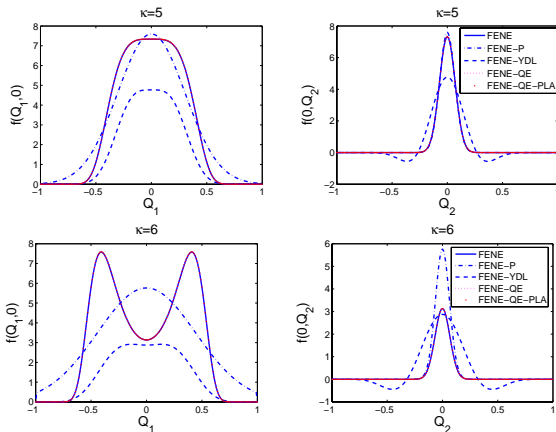


Figure: $f(Q_1, 0)$ (left) and $f(0, Q_2)$ (right) for $\kappa = 5$ and 6



Numerical results– elongational flow

κ	FENE-P	FENE-YDL	FENE-QE	FENE-QE-PLA
1	1.21×10^{-2}	1.64×10^{-2}	8.55×10^{-4}	8.55×10^{-4}
2	1.75×10^{-2}	7.39×10^{-2}	9.00×10^{-4}	9.00×10^{-4}
3	3.22×10^{-2}	1.88×10^{-1}	9.83×10^{-4}	9.83×10^{-4}
4	7.55×10^{-2}	3.83×10^{-1}	1.09×10^{-3}	1.09×10^{-3}
5	1.99×10^{-1}	6.62×10^{-1}	1.25×10^{-3}	1.23×10^{-3}
6	5.25×10^{-1}	9.93×10^{-1}	1.42×10^{-3}	1.42×10^{-3}
7	1.01×10^0	1.46×10^0	3.56×10^{-3}	1.73×10^{-3}
8	1.32×10^0	1.74×10^0	2.44×10^{-3}	2.44×10^{-3}

Table: Error of L1 norm of the CDFs



Numerical results– elongational flow

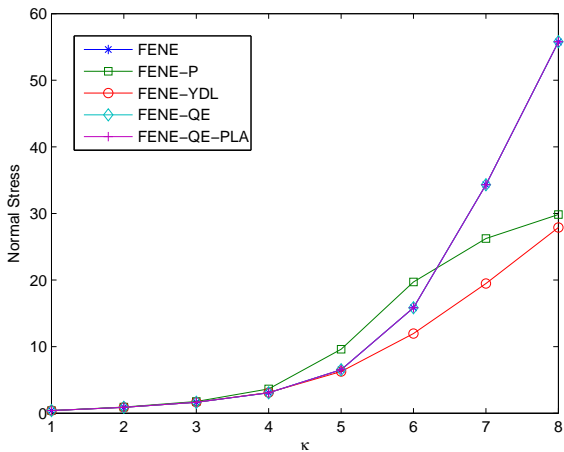


Figure: Comparison of the Normal Stress Difference



Numerical results– elongational flow

κ	FENE-P	FENE-YDL	FENE-QE	FENE-QE-PLA
1	9.25×10^{-3}	2.38×10^{-4}	3.33×10^{-5}	3.33×10^{-5}
2	3.32×10^{-2}	2.57×10^{-3}	7.01×10^{-5}	7.01×10^{-5}
3	1.25×10^{-1}	1.26×10^{-2}	1.44×10^{-4}	1.44×10^{-4}
4	5.90×10^{-1}	3.29×10^{-2}	2.29×10^{-4}	2.83×10^{-4}
5	3.07×10^0	2.69×10^{-1}	2.57×10^{-4}	1.59×10^{-4}
6	3.88×10^0	3.87×10^0	6.90×10^{-4}	6.34×10^{-4}
7	8.07×10^0	1.48×10^1	3.81×10^{-3}	1.95×10^{-3}
8	2.59×10^1	2.79×10^1	4.68×10^{-2}	4.68×10^{-2}

Table: Error of the Normal Stress Difference compared to Fokker-Planck equation



Numerical results– elongational flow

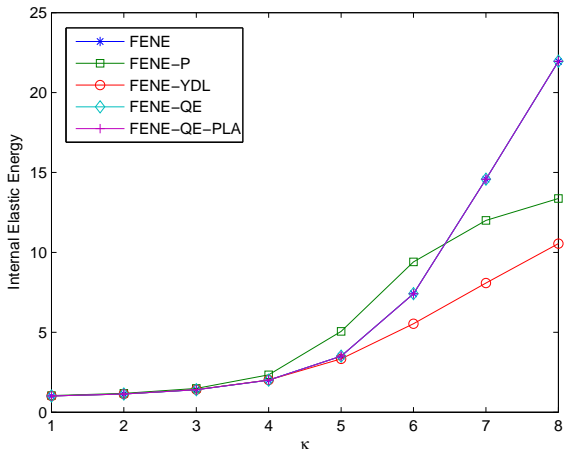


Figure: Comparison of the Elastic Energy



Numerical results– elongational flow

κ	FENE-P	FENE-YDL	FENE-QE	FENE-QE-PLA
1	2.47×10^{-2}	3.22×10^{-4}	3.53×10^{-5}	3.53×10^{-5}
2	4.51×10^{-2}	1.87×10^{-3}	5.20×10^{-5}	5.20×10^{-5}
3	8.32×10^{-2}	6.56×10^{-3}	8.86×10^{-5}	8.86×10^{-5}
4	3.35×10^{-1}	1.09×10^{-2}	1.20×10^{-4}	1.54×10^{-4}
5	1.56×10^0	1.68×10^{-1}	2.05×10^{-5}	9.33×10^{-6}
6	1.99×10^0	1.88×10^0	3.59×10^{-4}	3.28×10^{-4}
7	2.58×10^0	6.50×10^0	3.55×10^{-4}	6.38×10^{-4}
8	8.58×10^0	1.14×10^1	1.36×10^{-2}	1.36×10^{-2}

Table: Error of the elastic energy compared to Fokker-Planck equation



Numerical results– Lid driven cavity

Lid driven cavity

The simulation area is a 2-dimensional square cavity $[0, 1] \times [0, 1]$ whose top wall moves with a velocity distribution of

$$u(x, y = 1, t) = 16 \kappa a(t) x^2(1 - x)^2$$

Here κ is a constant and to start up the flow smoothly, $a(t)$ is chosen as a time dependent factor of

$$a(t) = \begin{cases} 0.1 t & 0 \leq t < 10 \\ 1 & t \geq 10 \end{cases}$$



Numerical results– Lid driven cavity

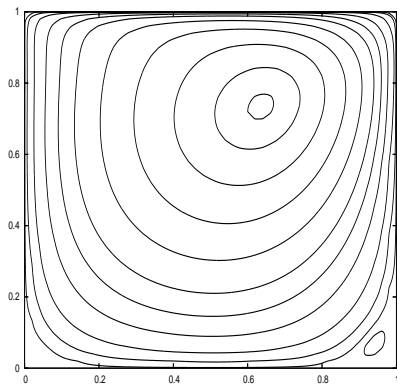


Figure: Stream line of lid-driven cavity, $\kappa = 1$ at $t = 40$



Numerical results– Lid driven cavity

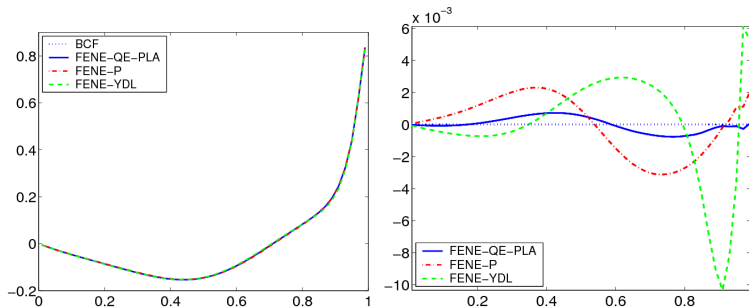


Figure: Horizontal velocity (left) and its error plot (right) on line $x = \frac{1}{2}$, $\kappa = 1$ at $t = 40$



Numerical results– Lid driven cavity

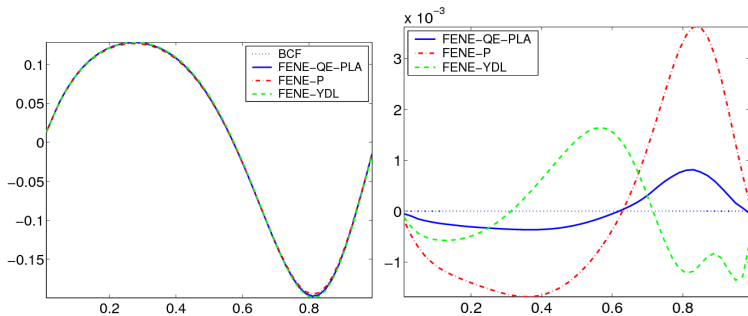


Figure: Vertical velocity (left) and its error plot (right) on line $y = \frac{1}{2}$, $\kappa = 1$ at $t = 40$



Numerical results

Computational cost comparison

model	homogeneous shear $\kappa = 20$	lid-driven cavity mesh 50×50 , $\kappa = 1$
FENE-QE	285s	
FENE-QE-PLA	< 1s	716s
FENE-P	< 1s	96s
FENE-YDL	< 1s	102s
BCF		$1.7 \times 10^4 \times 10$ s

Table: Computational cost comparison. Closure models are tested on a PC with a 3GHz Intel Pentium IV CPU. BCF ($N = 4000$) is run on ten 3.2GHz Intel Xeon CPUs.



Outline

Background

- Two approaches to tensor models

- Criteria of good closure approximations

- Quasi-equilibrium closure approximation (QEA)

FENE-QE Model

- FENE-QE model

- Implementation: FENE-QE-PLA

- Numerical results

Nonhomogeneous Kinetic Theories of LCPs

- Review of kinetic theories of LCPs

- Second-order moment model

- Fourth-order moment model

- Issue of implementation

- Numerical results of Bingham closure model

Conclusion and comments



System configuration

- assumption about macromolecules: rigid rod-like, very long.
- nonhomogeneous, configuration distribution function (CDF) depends on spatial variables and orientational variables:
 $f(\mathbf{x}, \mathbf{m}, t)$
- non-local intermolecular potential

$$U(\mathbf{x}, \mathbf{m}, t) = \int_{\Omega} \int_{|\mathbf{m}'|=1} G(\mathbf{x} - \mathbf{x}', \mathbf{m}, \mathbf{m}') f(\mathbf{x}', \mathbf{m}', t) d\mathbf{m}' d\mathbf{x}'.$$

- hydrodynamic-kinetic coupled incompressible isothermal system



Free energy

The free energy of the system is given by (for simplicity, kT is omitted)

$$A[f] = \int_{\Omega} \int_{|\mathbf{m}|=1} f \ln f + \frac{1}{2} f U d\mathbf{m} d\mathbf{x},$$

Then the chemical potential is

$$\mu = \frac{\delta A}{\delta f} = \ln f + U.$$



Kinetic equation

The equation for $f(\mathbf{x}, \mathbf{m}, t)$ reads

$$\frac{\partial f}{\partial t} + \mathbf{u} \cdot \nabla f = \nabla \cdot \left\{ [D_{\parallel} \mathbf{m} \mathbf{m} + D_{\perp} (I - \mathbf{m} \mathbf{m})] \cdot (f \nabla \mu) \right\} \\ + \mathcal{R} \cdot \left(D_r(\mathbf{m}) (f \mathcal{R} \mu) \right) - \mathcal{R} \cdot (\mathbf{m} \times \kappa \cdot \mathbf{m} f),$$

- D_{\parallel} , D_{\perp} : coefficients for translational diffusion parallel and perpendicular to the locale molecules orientation.
- $D_r(\mathbf{m})$ is coefficient for orientational diffusion.
- $\mathcal{R} = \mathbf{m} \times \partial / \partial \mathbf{m}$, $\kappa = (\nabla \mathbf{u})^T$.



Hydrodynamic equations

- continuity equation (assume ρ weak depends on $\nu = \langle 1 \rangle$)

$$\nabla \cdot \mathbf{u} = 0$$

- momentum equation

$$\rho \left[\frac{\partial \mathbf{u}}{\partial t} + (\mathbf{u} \cdot \nabla) \mathbf{u} \right] + \nabla p = \eta_s \Delta \mathbf{u} + \nabla \cdot \tau^s + \nabla \cdot \tau^e + \mathbf{F}^e,$$

η_s is the solvent viscosity, \mathbf{F}^e is body force, τ^e is polymer elastic stress, τ^s is polymer viscous stress.

$$\tau^s = \xi_r D : \langle \mathbf{m m m m} \rangle,$$

$D = (\kappa + \kappa^T)/2$ is the strain rate tensor, ξ_r is the coefficient of friction for solvent.



Elastic stress and body force

The elastic stress and body force read (virtual work principle)

$$\tau^e = -\langle \mathbf{m} \mathbf{m} \times \mathcal{R} \mu \rangle,$$

$$\mathbf{F}^e = - \int_{|\mathbf{m}|=1} \nabla U f(\mathbf{x}, \mathbf{m}, t) d\mathbf{m} = -\langle \nabla U \rangle.$$



Non-local excluded volume potential

We assume the mean-field intermolecular interaction takes form

$$G(\mathbf{x} - \mathbf{x}', \mathbf{m}, \mathbf{m}') = U_0 \frac{g(\mathbf{x}' - \mathbf{x}, \mathbf{m}) + g(\mathbf{x}' - \mathbf{x}, \mathbf{m}')}{2} |\mathbf{m} \times \mathbf{m}'|^2$$

$$g(\mathbf{x}' - \mathbf{x}, \mathbf{m}) = \frac{1}{\varepsilon_1 \varepsilon_2^2} g \left(\frac{|(\mathbf{x}' - \mathbf{x}) \cdot \mathbf{m}|^2}{\varepsilon_1^2} + \frac{|\mathbf{x}' - \mathbf{x}|^2 - |(\mathbf{x}' - \mathbf{x}) \cdot \mathbf{m}|^2}{\varepsilon_2^2} \right)$$

Some special form:

- In homogeneous system, leads to Maier-Saupe potential:

$$\begin{aligned} U_{MS}(\mathbf{m}, t) &= U_0 \int_{|\mathbf{m}'|=1} |\mathbf{m} \times \mathbf{m}'|^2 f(\mathbf{m}', t) d\mathbf{m}' \\ &= U_0 (\nu I - M) : \mathbf{m} \mathbf{m} \end{aligned}$$



Non-local excluded volume potential

- In nonhomogeneous system, can lead to Marrucci-Greco potential (weak distortion)

$$\begin{aligned} & U(\mathbf{x}, \mathbf{m}, t) \\ &= U_0 \left[(1 - c_1 \Delta)(\nu I - M) : \mathbf{m}\mathbf{m} + \frac{c_2}{2} \mathbf{m}\mathbf{m} : \nabla^2 (\nu I - M) : \mathbf{m}\mathbf{m} \right. \\ & \quad \left. + \frac{c_2}{2} \nabla^2 : (M I - Q) : \mathbf{m}\mathbf{m} \right] \end{aligned}$$

- isotropic long range interaction $\varepsilon_1 = \varepsilon_2 = \varepsilon$
(one-constant approximation)

$$g(\mathbf{x}' - \mathbf{x}, \mathbf{m}) = \frac{1}{\varepsilon^3} g\left(\frac{|\mathbf{x}' - \mathbf{x}|^2}{\varepsilon^2}\right) = g_\varepsilon(\mathbf{x}' - \mathbf{x})$$

$$U = U_0 g_\varepsilon * (\nu I - M) : \mathbf{m}\mathbf{m}$$



Energy dissipation

Energy dissipation of the hydrodynamic-kinetic coupled system

$$\begin{aligned} T \frac{dS}{dt} &= -\frac{d}{dt} \left(\int_{\Omega} \frac{1}{2} \rho \mathbf{u} \cdot \mathbf{u} dx + A[f] \right) \\ &= \int_{\Omega} \eta_s \nabla \mathbf{u} : \nabla \mathbf{u} + \xi_r \langle (\mathbf{m} \mathbf{m} : \kappa)^2 \rangle dx \\ &\quad + \int_{\Omega} \int_{|\mathbf{m}|=1} \left\{ D_r(\mathbf{m}) \mathcal{R}_{\mu} \cdot \mathcal{R}_{\mu} \right. \\ &\quad \left. + \nabla \mu \cdot [(D_{\parallel} - D_{\perp}) \mathbf{m} \mathbf{m} + D_{\perp} I] \cdot \nabla \mu \right\} f d\mathbf{m} dx \end{aligned}$$

It is non-negative provided:

$$\eta_s \geq 0, \quad \xi_r \geq 0, \quad D_{\parallel} \geq 0, \quad D_{\parallel} - D_{\perp} \geq 0, \quad D_r(\mathbf{m}) \geq 0.$$



Second-order moment model

$$\begin{aligned} \frac{dM}{dt} = & D_{\perp} \left[\Delta M + U_0 \nabla \cdot [\nabla(\nu I - M) * g_{\varepsilon} : Q] \right] \\ & + (D_{\parallel} - D_{\perp}) \left[\nabla \nabla : Q + U_0 \nabla \cdot [\nabla(\nu I - M) * g_{\varepsilon} : P] \right] \\ & - 2\bar{D}_r \left[(3M - \nu I) - U_0 (M * g_{\varepsilon} \cdot M + M \cdot M * g_{\varepsilon} - 2M * g_{\varepsilon} : Q) \right] \\ & + \kappa \cdot M + M \cdot \kappa^T - 2\kappa : Q \end{aligned}$$

$Q = \langle \mathbf{m}^4 \rangle$, $P = \langle \mathbf{m}^6 \rangle$. One-constant approximation and pre-average of $D_r(\mathbf{m})$ are adopted. Meanwhile the stress and body force can be expressed by moments,

$$\tau^e = (3M - \nu I) - U_0 (M \cdot M * g_{\varepsilon} + M * g_{\varepsilon} \cdot M - 2M * g_{\varepsilon} : Q),$$

$$\mathbf{F}^e = -\nabla(\nu I - M) * g_{\varepsilon} : M,$$

$$\tau^P = \xi_r \kappa : Q.$$



Second-order moment model – Bingham closure

Given M , we take the Bingham distribution as reference CDF

$$f_M(\mathbf{m}) = \frac{1}{z} \exp(\mathbf{m} \cdot B \cdot \mathbf{m}),$$

where B is a symmetric second order tensor. z is a normalized parameter. B , z are determined by

$$M = \int_{|\mathbf{m}|=1} f_M(\mathbf{m}) \mathbf{m} \mathbf{m} \, d\mathbf{m}$$

Q , P are approximated by

$$Q = \int_{|\mathbf{m}|=1} f_M(\mathbf{m}) \mathbf{m}^4 \, d\mathbf{m},$$

$$P = \int_{|\mathbf{m}|=1} f_M(\mathbf{m}) \mathbf{m}^6 \, d\mathbf{m}.$$



Second-order moment model – energy dissipation

The energy dissipation of the reduced model reads

$$\begin{aligned} T \frac{dS}{dt} &= -\frac{d}{dt} \left\{ \int_{\Omega} \frac{1}{2} \rho \mathbf{u} \cdot \mathbf{u} \, d\mathbf{x} + A[M] \right\} \\ &= \int_{\Omega} \left(\eta_s \nabla \mathbf{u} : \nabla \mathbf{u} + \xi_r \langle (\mathbf{m} \mathbf{m} : \kappa)^2 \rangle \Big|_{f=f_M} \right) d\mathbf{x} \\ &\quad + \int_{\Omega} \int_{|\mathbf{m}|=1} \left\{ \bar{D}_r \mathcal{R}\mu \cdot \mathcal{R}\mu \Big|_{f=f_M} \right. \\ &\quad \left. + \nabla \mu \cdot \left[(D_{\parallel} - D_{\perp}) \mathbf{m} \mathbf{m} + D_{\perp} I \right] \cdot \nabla \mu \Big|_{f=f_M} \right\} f_M \, d\mathbf{m} d\mathbf{x} \end{aligned}$$

It is non-negative provided

$$\eta_s \geq 0, \quad \xi_r \geq 0, \quad \bar{D}_r \geq 0, \quad D_{\perp} \geq 0, \quad D_{\parallel} - D_{\perp} \geq 0.$$



Fourth-order moment model

Fourth-order model for anisotropic long range potential

- Marrucci-Greco potential

$$U = \bar{U} :: \mathbf{m m m m}$$

$$\bar{U} = U_0 \left[(1 + c_1 \Delta)(\nu I - M)I + \frac{c_2}{2} (\nabla^2(\nu I - M) + \nabla^2 : (MI - Q)I) \right].$$

- Polymer stress

$$\begin{aligned} \tau^e = & \left[(3M - \nu I) + 4\bar{U}_{rsij} P_{rsijkl} - \bar{U}_{riij} Q_{rjkl} - \bar{U}_{rijj} Q_{rikl} \right. \\ & \left. - \bar{U}_{rijk} Q_{rijl} - \bar{U}_{rijl} Q_{rijk} \right], \end{aligned}$$

$$\tau^p = \xi_r \kappa : Q.$$

- Body force $\mathbf{F}^e = 0$, and the kinetic model satisfy energy dissipation.



Fourth-order moment model

$$\frac{dQ}{dt} = \frac{dQ_1}{dt} + \frac{dQ_2}{dt} + \frac{dQ_3}{dt}$$

$$\frac{dQ_1}{dt} = \nabla \cdot \left[D_{\perp} (\nabla Q + \nabla \bar{U} :: M_8) + (D_{\parallel} - D_{\perp}) (\nabla \cdot P + \nabla \bar{U} :: M_{10}) \right]$$

$$\frac{dQ_2}{dt} = \bar{D}_r \left[\langle \mathcal{R} \cdot \mathcal{R}(\mathbf{m m m m}) \rangle - \bar{U} :: \langle \mathcal{R}_i(\mathbf{m m m m}) \cdot \mathcal{R}_i(\mathbf{m m m m}) \rangle \right]$$

$$\frac{dQ_3}{dt} = -\kappa^T : \langle \mathbf{m m} \times \mathcal{R}(\mathbf{m m m m}) \rangle$$

$$\left[\frac{dQ_3}{dt} \right]_{ijkl} = 4\kappa_{rs} P_{rsijkl} - \kappa_{ri} Q_{rjkl} - \kappa_{rj} Q_{rik l} - \kappa_{rk} Q_{rijl} - \kappa_{rl} Q_{rijk}$$



Fourth-order moment model

Given Q , we take the reference CDF as

$$f_Q(\mathbf{m}) = \frac{1}{Z} \exp(\mathbf{m} \mathbf{m} : Y : \mathbf{m} \mathbf{m})$$

Y is a fourth-order symmetric tensor, and determined by

$$Q = \int_{|\mathbf{m}|=1} f_Q(\mathbf{m}) \mathbf{m} \mathbf{m} \mathbf{m} \mathbf{m} \, d\mathbf{m}$$

Then P, M_8, M_{10} are approximated by

$$P = \int_{|\mathbf{m}|=1} f_Q(\mathbf{m}) \mathbf{m}^6 \, d\mathbf{m} \quad M_8 = \int_{|\mathbf{m}|=1} f_Q(\mathbf{m}) \mathbf{m}^8 \, d\mathbf{m}$$
$$M_{10} = \int_{|\mathbf{m}|=1} f_Q(\mathbf{m}) \mathbf{m}^{10} \, d\mathbf{m}$$



Fourth-order moment model

The energy dissipation of the system reads

$$\begin{aligned} T \frac{dS}{dt} &= -\frac{d}{dt} \left(\int_{\Omega} \frac{1}{2} \rho \mathbf{u} \cdot \mathbf{u} d\mathbf{x} + A[Q] \right) \\ &= \int_{\Omega} \eta_s \nabla \mathbf{u} : \nabla \mathbf{u} + \xi_r \kappa : Q : \kappa d\mathbf{x} \\ &\quad + \int_{\Omega} \nabla \bar{\mu} :: \langle D_{\perp} \mathbf{m}^8 + (D_{\parallel} - D_{\perp}) \mathbf{m}^{10} \rangle |_{f=f_Q} :: (\nabla \bar{\mu})^T d\mathbf{x} \\ &\quad + \int_{\Omega} \bar{D}_r \bar{\mu} :: \langle \mathcal{R}_i(\mathbf{m} \mathbf{m} \mathbf{m} \mathbf{m}) \mathcal{R}_i(\mathbf{m} \mathbf{m} \mathbf{m} \mathbf{m}) \rangle |_{f=f_Q} :: \bar{\mu}^T d\mathbf{x}, \end{aligned}$$

where $\bar{\mu} = Y - \ln z H + \bar{U}$.

It is non-negative, provided $\eta_s \geq 0$, $\xi_r \geq 0$, $\bar{D}_r \geq 0$, $D_{\perp} \geq 0$ and $D_{\parallel} - D_{\perp} \geq 0$.



Issue of implementation

- Efficient algorithms of evaluating $Q(M), P(M)$ according to Bingham closure are needed to make the closure approximation practical
- Legendre integrator scheme of Ilg et al (2000, 2003) is not efficient enough for nonhomogeneous simulation
- Fortunately, $Q(M), P(M)$ are not depended on the dynamics. There are two approaches to evaluate them



Issue of implementation – Bingham closure

- Evaluating in local coordinate system [Chaubal and Leal 1998]

$$M = \text{Diag}(s_1, s_2, 1 - s_1 - s_2), \quad B = \text{Diag}(l_1, l_2, 1 - l_1 - l_2).$$

Q has 6 non-zero components:

$$Q_{1111}, Q_{2222}, Q_{3333}, Q_{1122}, Q_{1133}, Q_{2233},$$

but only 3 are independent, because of $\sum_j Q_{ijij} = M_{ii} = s_i$
Fit $Q_{1111}, Q_{2222}, Q_{3333}$ by polynomials of s_1, s_2 :

$$Q_{iiii} = k_0 + k_1 s_1 + k_2 s_1^2 + k_3 s_1^3 + \dots + k_9 s_1 s_2^2.$$

the coefficients k_i determined by least-square method, while Q_{iiii}, s_1, s_2 are obtained by integral on given (l_1, l_2) samples.



Issue of implementation – Bingham closure

- Explicit form [Grosso et al 2000]. A general expression of Q in terms of M :

$$\begin{aligned} Q_{ijkl} = & \beta_1 \mathcal{G}(\delta_{ij} \delta_{kl}) + \beta_2 \mathcal{G}(\delta_{ij} M_{kl}) + \beta_3 \mathcal{G}(M_{ij} M_{kl}) \\ & + \beta_4 \mathcal{G}(\delta_{ij} M_{km} M_{ml}) + \beta_5 \mathcal{G}(M_{ij} M_{km} M_{ml}) \\ & + \beta_6 \mathcal{G}(M_{im} M_{mj} M_{kn} M_{nl}) \end{aligned}$$

where \mathcal{G} is symmetrization operator

$$\mathcal{G}(X_{ijkl}) = \frac{1}{24}(X_{ijkl} + X_{ijlk} + \dots).$$

β_i depend on the two independent invariants of M :

$$I_2 = \frac{1}{2}(1 - M : M), \quad I_3 = \det(M).$$

and β_i are fitted by polynomials with least-square method.



Issue of implementation – Bingham closure

- These two approaches could be extended to higher-order quasi-equilibrium closure approximation
- Employ piecewise linear approximation (PLA) or other numerical skills if $Q(M)$, $P(M)$ are singular in some special system



Numerical results of Bingham closure model

- Bingham closure agrees with the exact kinetic theory qualitatively for homogeneous and nonhomogeneous system, except for its failure to predict flow-aligning at high Deborah number and high nematic potential strength
- It agrees with the exact kinetic theory quantitatively when nematic potential strength is in the middle region.
- The position of homoclinic bifurcation predicted by Bingham closure is different with the exact kinetic theory in two-dimensional problem. The difference is not clear in three-dimensional problem.
- In general, Bingham closure is more accurate than other closures, e.g. Doi's quadratic closure, HL1, HL2 etc



Homogeneous bifurcation diagram

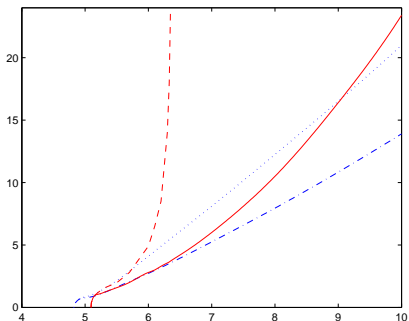


Figure: The horizontal axis is nematic potential strength U_0 ; the vertical axis is the Deborah number De . Blue lines are of exact kinetic theory, Red lines are of Bingham closure.



Nonhomogeneous results

Bingham closure can predict the five modes of director configurations in Couette flow as exact kinetic model

- (a) ES: elastic-driven steady state
- (b) T: tumbling state
- (c) TWD: tumbling-wagging composite with inside defects
- (d) W: wagging state
- (e) VS: viscous-driven steady state



Modes of director dynamics

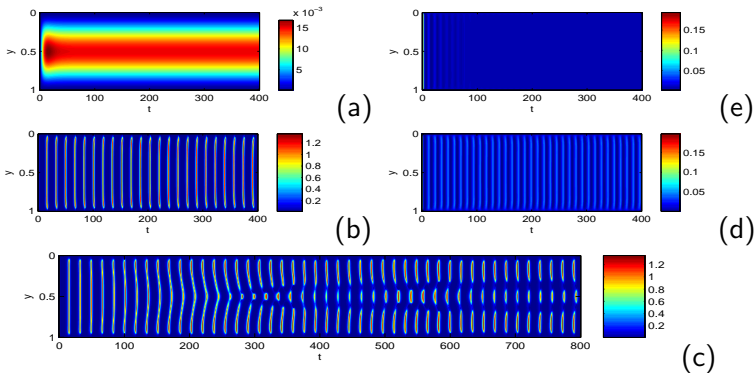


Figure: Five flow modes. Colors represent the director angle. The horizontal axis is dimensionless time and the vertical axis is the distance to lower slab. The parameters are $U_0 = 6$ (a) $De = 0.01$; (b) $De = 1.0$; (c) $De = 2.0$; (d) $De = 4.0$; (e) $De = 6.0$.



Defect dynamics

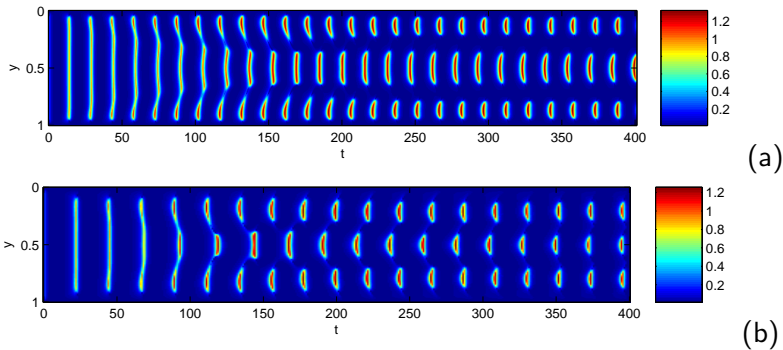


Figure: Typical TWD modes in Couette flow at $U_0 = 5.5$, $De = 1.5$. (a) exact kinetic model, (b) Bingham closure. Colors represent the director angle. The horizontal axis is dimensionless time and the vertical axis is the distance to lower slab.



Defect dynamics in Poiseuille flow

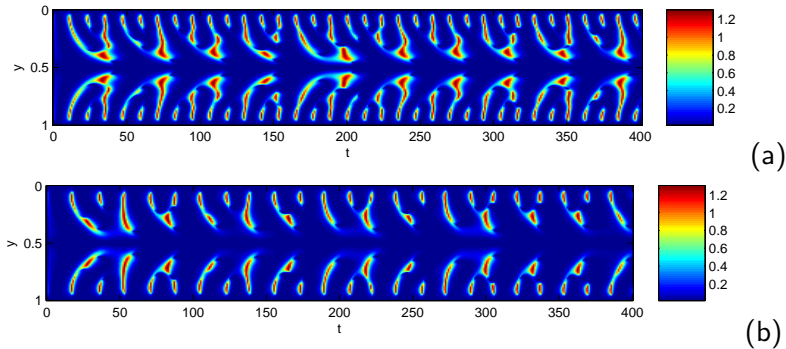


Figure: Typical orientational configuration in Poiseuille flow. $U_0 = 5.5$, $De = 1.0$. (a) exact kinetic model, (b) Bingham closure. Colors represent the director angle. The horizontal axis is dimensionless time and the vertical axis is the distance to lower slab.



Error of Bingham closure

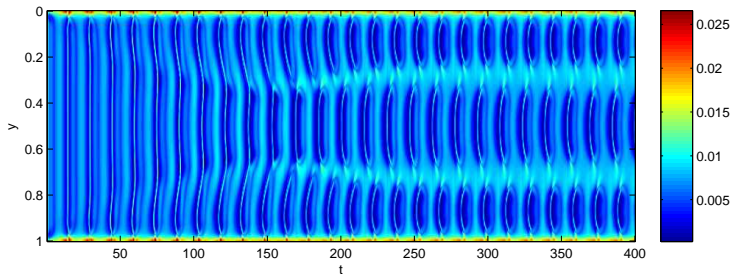


Figure: The error of Bingham closure in every time step of exact kinetic simulation. $U_0 = 5.5$, $De = 1.5$. The horizontal axis is dimensionless time and the vertical axis is the distance to lower slab. Colors represent the total error of five components of Q evaluated by Bingham closure



Outline

Background

- Two approaches to tensor models

- Criteria of good closure approximations

- Quasi-equilibrium closure approximation (QEA)

FENE-QE Model

- FENE-QE model

- Implementation: FENE-QE-PLA

- Numerical results

Nonhomogeneous Kinetic Theories of LCPs

- Review of kinetic theories of LCPs

- Second-order moment model

- Fourth-order moment model

- Issue of implementation

- Numerical results of Bingham closure model

Conclusion and comments



Conclusion and comments

- We present four criteria for closure approximations.
- Quasi-equilibrium closure approximation of FENE model (FENE-QE) satisfies the first three criteria
- Piecewise linear approximation is introduced to reduce the computational cost of FENE-QE without losing accuracy
- A general nonhomogeneous model of LCPs is presented. And reduced moments models keeping energy dissipation are proposed by quasi-equilibrium closure
- The second-order Bingham closure model agrees with the exact nonhomogeneous kinetic model qualitatively, except for the failure to predict flow-aligning when nematic potential strength and Deborah number are very high
- The closure problem of kinetic models of LCPs are more difficult than FENE model of dumbbell polymer (nonlinear, phase transition). Higher-order tensor models are needed to give more accurate results



The End

Thank You !



Appendix A

The HL1 and HL2 closures (Hinch and Leal 1976)

- HL1

$$B : Q = \frac{1}{5} [6M \cdot B \cdot M - B : MM + 2I(M - M \cdot M) : B]$$

- HL2

$$B : Q = MM : B + 2M \cdot B \cdot M - \frac{M \cdot M : (\kappa + \kappa^T)}{M : M} M \cdot M \\ + \rho \left[\frac{52}{315} B - \frac{8}{21} \left(B \cdot M + M \cdot B - \frac{2}{3} (A : M) I \right) \right]$$

where $\rho = \exp[(2 - 6M : M)/(1 - M : M)]$.

In this two equation, B is any traceless tensor. Q is fourth-order moment of CDF. [▶ go back](#)



Appendix B

Energy dissipation of Bingham closure model of LCPs

Definition of free energy

$$\begin{aligned} A[M] &= \int_{\Omega} \int_{|\mathbf{m}|=1} f_M \ln f_M + \frac{1}{2} U f_M d\mathbf{m} dx \\ &= \int_{\Omega} (B - \ln z I) : M + \frac{U_0}{2} g_{\varepsilon} * (\nu I - M) : M dx. \end{aligned}$$

The chemical potential under reference CDF reads

$$\mu_M = \bar{\mu}_M : \mathbf{m}\mathbf{m},$$

where $\bar{\mu}_M = (B - \ln z I) + \bar{U}_M$ and $\bar{U}_M = U_0 g_{\varepsilon} * (\nu I - M)$



Appendix B

Calculate the energy dissipation

$$\begin{aligned} T \frac{dS}{dt} &= - \frac{d}{dt} \left\{ \int_{\Omega} \frac{1}{2} \rho \mathbf{u} \cdot \mathbf{u} d\mathbf{x} + A[M] \right\} \\ &= - \int_{\Omega} \rho \mathbf{u} \cdot \mathbf{u}_t d\mathbf{x} - \int_{\Omega} \frac{d}{dt} (B - \ln zI) : M d\mathbf{x} \\ &\quad - \int_{\Omega} (B - \ln zI) : \frac{dM}{dt} + \frac{U_0}{2} \frac{d}{dt} [\bar{U}_M : M] d\mathbf{x} \\ &= - \int_{\Omega} \mathbf{u} \cdot [\eta_s \Delta \mathbf{u} + \nabla \cdot \boldsymbol{\tau}^s + \nabla \cdot \boldsymbol{\tau}^e + \mathbf{F}^e - \nabla p] d\mathbf{x} \\ &\quad - \int_{\Omega} \frac{d\nu}{dt} d\mathbf{x} - \int_{\Omega} \bar{\mu}_M : \frac{dM}{dt} d\mathbf{x} \\ &\quad - \frac{U_0}{2} \int_{\Omega} \frac{d}{dt} \bar{U}_M : M - \bar{U}_M : \frac{dM}{dt} d\mathbf{x} \end{aligned}$$



Appendix B

$$\begin{aligned} &= \int_{\Omega} \eta_s \nabla \mathbf{u} : \nabla \mathbf{u} + \xi_r \kappa : \mathbf{Q} : \kappa \, d\mathbf{x} \\ &\quad + 2\bar{D}_r \int_{\Omega} (\bar{\mu}_M)_{ij} (\delta_{ik} M_{lj} + M_{il} \delta_{kj} - 2Q_{ijkl}) (\bar{\mu}_M)_{kl} \, d\mathbf{x} \\ &\quad + \int_{\Omega} \nabla \bar{\mu}_M : \left((D_{\parallel} - D_{\perp}) P + D_{\perp} \langle \mathbf{m} \mathbf{m} / \mathbf{m} \mathbf{m} \rangle \right) : (\nabla \bar{\mu}_M)^T \, d\mathbf{x} \end{aligned}$$

It is non-negative provided $\eta_s > 0$, $\xi_r > 0$, $\bar{D}_r > 0$, $D_{\perp} > 0$ and $D_{\parallel} - D_{\perp} > 0$.

In the calculation, Identity $(B - \ln z I)_t : M = \nu_t$ and mass conservation $\int_{\Omega} \nu \, d\mathbf{x} = \text{Constant}$ are employed.



Appendix C

Energy dissipation of fourth-order tensor model of LCPs

$$\begin{aligned}
 A[Q] &= \int_{\Omega} \int_{|\mathbf{m}|=1} f_y \ln f_y + \frac{1}{2} f_y U \, d\mathbf{m} \, d\mathbf{x} \\
 &= \int_{\Omega} (Y - \ln z||) :: Q + \frac{1}{2} \bar{U} :: Q \, d\mathbf{x}
 \end{aligned}$$

$$\begin{aligned}
 T \frac{dS}{dt} &= -\frac{d}{dt} \left(\int_{\Omega} \frac{1}{2} \rho \mathbf{u} \cdot \mathbf{u} \, d\mathbf{x} + A[Q] \right) \\
 &= -\int_{\Omega} \rho \mathbf{u} \cdot \mathbf{u}_t \, d\mathbf{x} - \int_{\Omega} (Y - \ln z||) :: \frac{dQ}{dt} + \frac{1}{2} \frac{d}{dt} (\bar{U} :: Q) \, d\mathbf{x} \\
 &= \int_{\Omega} \eta_s \nabla \mathbf{u} : \nabla \mathbf{u} + \xi_r \kappa : Q : \kappa \, d\mathbf{x} \\
 &\quad + \int_{\Omega} \nabla \bar{\mu} :: \left[D_{\perp} M_8 + (D_{\parallel} - D_{\perp}) M_{10} \right] :: (\nabla \bar{\mu})^T \, d\mathbf{x} \\
 &\quad + \int_{\Omega} \bar{D}_r \bar{\mu} :: \langle \mathcal{R}_i(\mathbf{m}\mathbf{m}\mathbf{m}\mathbf{m}) \mathcal{R}_i(\mathbf{m}\mathbf{m}\mathbf{m}\mathbf{m}) \rangle :: \bar{\mu}^T \, d\mathbf{x}
 \end{aligned}$$

